A Novel Synthesis for Bandwidth Switchable Bandpass Filters Using Semi-conductor Distributed Doped Areas

Rozenn Allanic, Denis Le Berre, Yves Quéré, Cédric Quendo, David Chouteau, Virginie Grimal, Damien Valente, Jérôme Billoue

▶ **To cite this version:**

Rozenn Allanic, Denis Le Berre, Yves Quéré, Cédric Quendo, David Chouteau, et al.. A Novel Synthesis for Bandwidth Switchable Bandpass Filters Using Semi-conductor Distributed Doped Areas. IEEE Access, 2020, pp.1-1. 10.1109/ACCESS.2020.3006709 . hal-02889751

HAL Id: hal-02889751
https://hal.science/hal-02889751v1

Submitted on 11 Oct 2024

HAL is a multi-disciplinary open access archive for the deposit and dissemination of scientific research documents, whether they are published or not. The documents may come from teaching and research institutions in France or abroad, or from public or private research centers.

L'archive ouverte pluridisciplinaire **HAL**, est destinée au dépôt et à la diffusion de documents scientifiques de niveau recherche, publiés ou non, émanant des établissements d'enseignement et de recherche français ou étrangers, des laboratoires publics ou privés.

Distributed under a Creative Commons Attribution 4.0 International License

IEEE Access
Multidisciplinary ⋮ Rapid Review ⋮ Open Access Journal

Received April 24, 2020, accepted June 23, 2020, date of publication July 2, 2020, date of current version July 16, 2020.

Digital Object Identifier 10.1109/ACCESS.2020.3006709

A Novel Synthesis for Bandwidth Switchable Bandpass Filters Using Semi-Conductor Distributed Doped Areas

ROZENN ALLANIC[1], (Member, IEEE), DENIS LE BERRE[1], (Member, IEEE), YVES QUERE[1], (Member, IEEE), CÉDRIC QUENDO[1], (Senior Member, IEEE), DAVID CHOUTEAU[2], VIRGINIE GRIMAL[2], DAMIEN VALENTE[2], AND JÉRÔME BILLOUE[2]

[1]Laboratoire des Sciences et Techniques de l'Information, de la Communication et de la Connaissance (Lab-STICC), Université de Brest, 29238 Brest, France
[2]Laboratoire GREMAN, Université de Tours, 37071 Tours, France

Corresponding author: Rozenn Allanic (rozenn.allanic@univ-brest.fr)

This work was supported in part by the French CERTeM Technological Platform, in part by the European Union through the European Regional Development Fund (ERDF), and in part by the Ministry of Higher Education and Research and Brittany Region, through the CPER Project SOPHIE/STIC and ONDES.

ABSTRACT This paper presents a novel synthesis for bandwidth switchable bandpass filters using Semi-conductor Distributed Doped Areas (ScDDAs) as active elements. A co-design method is proposed with a global and simultaneous conception for the active and the passive parts of the switchable filters. The ScDDAs, integrated in the silicon substrate, are able to commute from half-wavelength open-ended stubs to quarter-wavelength short-circuited ones. This co-design method offers a great flexibility and allows to integrate the active elements directly in the substrate, therefore avoiding any soldering of components. The synthesis is developed for the two-states of the active elements and applied, as a proof of concept, to a four-pole bandwidth switchable bandpass filter. This filter operates at 5 GHz with a 50 % bandwidth in the OFF-state (when the stubs are terminated by an open-circuit) and with a 70 % bandwidth in the ON-state (when the stubs are short-circuited). For this filter, the synthesis is detailed in the two-states allowing to choose the two desired bandwidths. A good fitting is obtained for these results proving the viability of such an approach.

INDEX TERMS Bandpass filter (BPF), bandwidth tunability, co-design, discrete tuned, filter synthesis, reconfigurable filter, ScDDA, tunable filter.

I. INTRODUCTION

The digital society is in perpetual evolution and thus needs to deal with some major technological challenges that affect the microwave devices performances which are widely used in the telecommunications systems and for Internet-of-Things applications. Switches, filters or antennas in the transmitter-receivers have always to complete the same tradeoffs in terms of size, cost, power handling and electrical and thermal performances. Therefore, in the last few years more and more studies led to new ways to design microwave functions in a global approach instead of a component-by-component approach. Some studies [1]–[3] present co-designs of filtering-antennas in order to reach the best tradeoffs for a raise in frequency. Moreover, some switchable filtering-antennas use a reconfigurable bandwidth filter [4], [5] to commute from ultra wideband to narrowband and therefore modify the antenna selectivity. Taking into account the environment of microwave components is also a subject of interest for the co-design of RF components, such as Radio Frequency IDentification (RFID) antennas and its environment [6]. Furthermore, the technological challenges become more prevalent when it comes to a global design with active and passive components added to other components such as a fully integrated Voltage Controlled Oscillator (VCO) [7], or to a Single Pole Double Throw (SPDT) type switch associated to a Low Noise Amplifier (LNA) to obtain an ultra-low noise co-designed SPDT-LNA [8]. In this way, it is

The associate editor coordinating the review of this manuscript and approving it for publication was M. Saif Islam.

This work is licensed under a Creative Commons Attribution 4.0 License. For more information, see https://creativecommons.org/licenses/by/4.0/

necessary to compute a global analysis such as with full wave and time domain descriptions for microwave receivers and converters for RFID [9], or with nonlinear analysis techniques and electromagnetic simulations for a transmitter consisting in an antenna and a doubly balanced Field Effect Transistor (FET) mixer [10]. These entire co-design approaches aim to optimize the whole system performances, homogenize the technology, minimize the interconnection problems and reduce the system size and therefore the cost. To go further, a co-simulation tool allows to predict an accurate system behavior simulated to minimize the return trips between the research and the fabrication and, consequently, to reduce the prototyping cost.

Thus, in order to succeed in moving towards efficient and miniature communicating systems, it is necessary to make several functionalities where different standards coexist on the same chip. In the case of filters, many solutions exist to do so: a first solution consists in multiplying the components, such as filter banks [11], by the targeted standards number, the performances of each device can be optimized but it is at the detriment of the size and the cost. A second solution is to address a switchable frequency band with RF switches such as Micro-ElectroMechanical Systems (MEMS) [12]–[15], PIN diodes [16]–[21] or FET transistors [22].

However, active components are getting smaller and smaller when the microstrip transmission lines are still wider than the Surface Mounted Devices (SMDs). Soldering these components on the substrate leads to some parasitic effects, caused by mismatches at the interconnections level and by the size difference between the passive and the active parts. These SMDs are widely used in bandpass filters with reconfigurable bandwidths [23]–[27], however they limit the rise in frequency in such reconfigurable applications. Moreover, in microstrip technology, active components are linked to the ground using metallized via-holes (to connect the DC and RF grounds) to ensure biasing. These via-holes add additional losses and parasitic effects. Consequently, in a tunable microwave function, a global design approach permits no more to optimize the active component and the passive device separately but the entire tunable function to focus on the final performances.

In this way, some previous studies show the possibility to co-design simultaneously the two parts of a tunable microwave device [28]–[30]. The passive part is designed on a High-Resistivity Silicon (HR-Si) substrate to minimize the losses and the active elements are based on Semi-conductor Distributed Doped Areas (ScDDAs), so they are integrated in the substrate. In this context, a three-state tunable resonator [31] shows the flexibility in co-designing two active elements and the passive component in the same design flow. The active elements are made with some N^+PP^+ junctions with two different sizes, integrated in the substrate, and, thanks to this approach, a unique DC source is needed to commute the two active elements offering to the resonator three working states.

Therefore, this approach offers a great flexibility, a low switching voltage, a unique DC source to control different junctions and a very simple manufacturing process (the same as for the semiconductor components with only two masks). In addition to that, interconnections and parasitic effects due to size mismatches are no longer a problem for such devices. To go further in this direction, a ScDDA has been designed in a triangle shape as an active element for a tunable resonator in order to achieve a continuous tuning and reach a 50 % resonant frequency variation [32]. Moreover, the use of a HR-Si substrate allows to design low-losses RF filters [33] and presents some constant performances on a large temperature range [34].

In that respect, the idea of this work is to take advantage of the co-design flexibility with ScDDAs as active elements to design switchable bandpass filters and to target in future works a co-design of switchable filtering-antenna.

This paper is organized as follow. First, in Section II, the synthesis of the filter is presented and the bandwidths range is illustrated by examples of four-pole bandwidth switchable bandpass filters. Then, in Section III, the fabrication process is described before explaining in Section IV the co-simulation method between the electrical characteristics of the active element and the propagating wave of the passive parts. Finally, in Section V, a 5 GHz four-pole bandwidth switchable bandpass filter is proposed as a demonstrator and its characterization validates the method.

II. SYNTHESIS OF THE BANDWIDTH SWITCHABLE BANDPASS FILTER

The idea of this paper is to develop a novel synthesis for bandwidth switchable bandpass filters with two working states and therefore two different bandwidths. The starting points of the novel synthesis are the quarter-wavelength short-circuited stubs synthesis with constant impedance and the half-wavelength open-circuited stubs synthesis with stepped-impedance [35], which are detailed in the first two parts of this section. The simplified layout of these two filters are presented in Fig. 1 (a) and (b).

Then, in this paper, the idea is to adapt these syntheses to the novel one detailed in the last part of this section, allowing to choose the two bandwidths of a bandwidth switchable bandpass filter. The filter is designed with half-wavelength open-circuited stubs, and some active elements are used for the commutation from half-wavelength open-circuited stubs, in the OFF-state, to quarter-wavelength short-circuited stubs in the ON-state (Fig. 1 (c)).

A. QUARTER-WAVELENGTH SHORT-CIRCUITED STUBS

Fig. 2 shows the circuit design of a bandpass filter with short-circuited terminations, using impedances determined from Matthaei's book [35].

First, the electrical length, θ_1, and the inverter admittances of the bandpass filter can be calculated using (1) to (5) with ω_1 the bandwidth, Y_A the characteristic admittance.

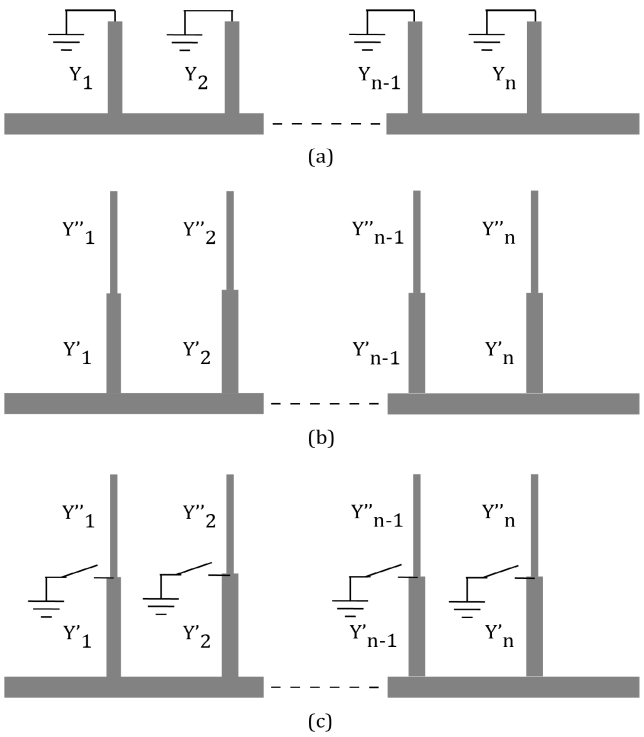

FIGURE 1. Ideal layout of a N-pole bandpass filter (a) with quarter-wavelength short-circuited stubs and constant impedance. (b) with half-wavelength open-circuited stubs with stepped- impedance. (c) with half-wavelength open-circuited stubs with stepped- impedance able to commute to quarter-wavelength short-circuited stubs.

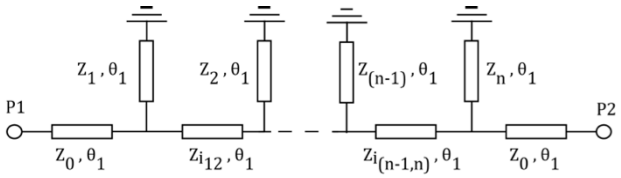

FIGURE 2. Design of an N-pole bandpass filter with short-circuited terminations.

d is a constant parameter which can be chosen between 0 and 1 to have the best admittances for the filter, *i.e.* a tradeoff between the impedances of the stubs, which have lower parasitic effects if their values are not very different, and most of all impedance values, which take into account the manufactured constraints linked to the chosen technology.

The element values $g_0, g_1, \ldots, g_n, g_{n+1}$ are the coefficient of the low-pass prototype Tchebyscheff filter and the parameter ω_1' is the radian frequency of the pass-band edge, which is set to 1. The bandwidth is calculated at the ripple.

$$\theta_1 = \frac{\pi}{2}\left(1 - \frac{\omega_1}{2}\right) \tag{1}$$

$$\frac{J_{12}}{Y_A} = g_0\sqrt{\frac{C_a}{g_2}} \tag{2}$$

$$\left.\frac{J_{k,k+1}}{Y_A}\right|_{k=2 \text{ to } n-2} = \frac{g_0 C_a}{\sqrt{g_k g_{k+1}}} \tag{3}$$

$$\frac{J_{n-1,n}}{Y_A} = g_0\sqrt{\frac{C_a g_{n+1}}{g_0 g_{n-1}}} \tag{4}$$

$$C_a = 2dg_1 \tag{5}$$

Then, the characteristics admittances of the short-circuited stubs can be computed using (6) to (9). The characteristics admittances of the inverters can be evaluated with (10).

$$\left.N_{k,k+1}\right|_{k=1 \text{ to } n-1} = \sqrt{\left(\frac{J_{k,k+1}}{Y_A}\right)^2 + \left(\frac{g_0\omega_1' C_a \tan\theta_1}{2}\right)^2} \tag{6}$$

$$Y_1 = g_0 Y_A \omega_1'(1-d) g_1 \tan\theta_1 + Y_A\left(N_{12} - \frac{J_{12}}{Y_A}\right) \tag{7}$$

$$\left.Y_k\right|_{k=2 \text{ to } n-1} = Y_A\left(N_{k-1,k} + N_{k,k+1} - \frac{J_{k-1,k}}{Y_A} - \frac{J_{k,k+1}}{Y_A}\right) \tag{8}$$

$$Y_n = Y_A\omega_1'\left(g_n g_{n+1} - d g_0 g_1\right)\tan\theta_1 + Y_A\left(N_{n-1,n} - \frac{J_{n-1,n}}{Y_A}\right) \tag{9}$$

$$\left.Yi_{k,k+1}\right|_{k=1 \text{ to } n-1} = Y_A\left(\frac{J_{k,k+1}}{Y_A}\right) \tag{10}$$

Using (11) to (13), the short-circuited quarter-wavelength stubs characteristic admittances can be simplified using (14).

$$\alpha_1 = g_0\omega_1'\left(1 - d\right) g_1 \tan\theta_1 + \left(N_{12} - \frac{J_{12}}{Y_A}\right) \tag{11}$$

$$\left.\alpha_k\right|_{k=2 \text{ to } n-1} = \left(N_{k-1,k} + N_{k,k+1} - \frac{J_{k-1,k}}{Y_A} - \frac{J_{k,k+1}}{Y_A}\right) \tag{12}$$

$$\alpha_n = \omega_1'\left(g_n g_{n+1} - d g_0 g_1\right)\tan\theta_1 + \left(N_{n-1,n} - \frac{J_{n-1,n}}{Y_A}\right) \tag{13}$$

$$\left.Y_k\right|_{k=1 \text{ to } n} = Y_A\alpha_k \tag{14}$$

B. HALF-WAVELENGTH OPEN-CIRCUITED STUBS WITH STEPPED-IMPEDANCE

This filter can be synthesis using half-wavelength stepped-impedance open-circuited stubs. First of all, one should note that the characteristic admittances of the inverters are calculated using the same equation as the previous ones. Then, inner quarter wavelength portion can be determined using (15).

$$\left.Y_k'\right|_{k=1 \text{ to } n} = Y_k\left(\frac{a_k \tan^2\theta_1 - 1}{\tan^2\theta_1\left(a_k + 1\right)}\right) \tag{15}$$

Next, the second portion of the stubs can be calculated with (16).

$$\left.Y_k''\right|_{k=1 \text{ to } n} = a_k Y_k' \tag{16}$$

where the parameter a_k, the ratio of the transmission zero by the resonant frequency, is defined by (17).

$$a_k = \cot^2\left(\frac{\pi\omega_\infty}{2\omega_0}\right)\Bigg|_{(\omega_\infty/\omega_0)<(\omega_1/\omega_0)} \tag{17}$$

C. HALF-WAVELENGTH OPEN-CIRCUITED STUBS WITH STEPPED-IMPEDANCE SWITCHABLE TO QUARTER-WAVELENGTH SHORT-CIRCUITED STUBS

Thanks to the two previous syntheses given in [35], new equations unifying the two syntheses are given in this part

offering the possibility to choose the two bandwidths of the reconfigurable filter; a_k is now used as a flexibility parameter in the bandwidths calculation instead of being the ratio of the transmission zero frequency and the resonant frequency. Based on the synthesis of quarter-wavelength short-circuited stubs, the first bandwidth is ω_1.

Then, the idea is to short-circuit the stepped-impedance stubs at the end of the inner quarter-wavelength portion, *i.e.* at the stepped-impedance transition, therefore, the first inner characteristic impedance can be determined by (18) using (14).

$$Y'_k\big|_{k=1\ \text{to}\ n} = Y_k \tag{18}$$

Then, using the synthesis of half-wavelength open-circuited stubs the bandwidth is ω_2 and the equation (1) is replaced by (19) and allows to calculate α'_k with θ_2 in the equations from (6) to (9).

$$\theta_2 = \frac{\pi}{2}\left(1 - \frac{\omega_2}{2}\right) \tag{19}$$

This leads to determine a_k in (16) with (20) for the second portion of the stubs.

$$a_k\big|_{k=1\ \text{to}\ n} = \left(\frac{\tan^2\theta_2\alpha_k + \alpha'_k}{\tan^2\theta_2\left(\alpha'_k - \alpha_k\right)}\right) \tag{20}$$

Finally, the synthesis ends to the calculation of the stub impedances of each filter transmission line, and this using (21) to (23), with *Zi* the inverter impedance, *Zp* the first part of the stubs and *Zs* the second part of the stubs. Fig. 3 (a) and (b) present the ideal designs of an N-pole switchable bandpass filter in the OFF-state and the ON-state, respectively.

$$Zi_{k,k+1}\big|_{k=1\ \text{to}\ n-1} = \frac{1}{Yi_{k,k+1}\big|_{k=1\ \text{to}\ n-1}} \tag{21}$$

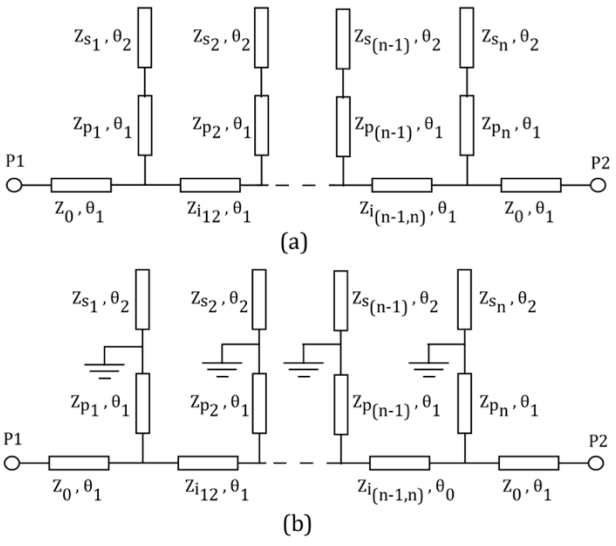

FIGURE 3. Ideal designs of an N-pole switchable bandpass filter. (a) in the OFF-state. (b) in the ON-state.

$$Zp_k\big|_{k=1\ \text{to}\ n} = \frac{1}{Y'_k\big|_{k=1\ \text{to}\ n-1}} \tag{22}$$

$$Zs_k\big|_{k=1\ \text{to}\ n} = \frac{1}{Y''_k\big|_{k=1\ \text{to}\ n-1}} \tag{23}$$

Therefore, ω_2 is the chosen bandwidth for the OFF-state when the resonators are open-circuited and ω_1 is the chosen bandwidth for the ON-state when the resonators are short-circuited at the stepped-impedance position.

D. SWITCHABLE EXAMPLES

Using the ideal designs of Fig. 3, with the element values for a Tchebyscheff filter and the two chosen bandwidths, the synthesis allows to calculate the impedances of each transmission line, and each length depends on the chosen center frequency.

As examples, four-pole bandpass filters have been simulated with ADS© from Keysight Technologies in microstrip technology thanks to the synthesis to give an overview of the bandwidth couples. The element values for a four-pole Tchebyscheff filter are listed in Table 1.

TABLE 1. Element values for a Tchebyscheff filter for a 0.01 db ripple.

n	g_0	g_1	g_2	g_3	g_4	g_5	ω'_1
4	1	0.7128	1.2003	1.3212	0.6476	1.1007	1

Fig. 4 presents two simulated results of bandpass filters which operate at 5 GHz, with a 15 % relative bandwidth in the OFF-state and a 45 % relative bandwidth in the ON-state (Fig. 4 (a)) and with a 61 % relative bandwidth in the OFF-state and a 94 % relative bandwidth in the ON-state (Fig. 4 (b)). In the OFF-state, the resonators are open-circuited whereas in the ON-state the resonators are short-circuited at the stepped-impedance position. These simulated results are just some illustrations of the bandwidth choice flexibility offered by the synthesis, but, of course, some limitations appear with the technology in the impedance values despite the freedom degree, *d*, in the synthesis. Therefore, Table 2 gives impedance characteristic range examples depending on the bandwidths couples chosen.

TABLE 2. Impedances range given by the synthesis depending on the bandwidths choice and the freedom degree d.

ω_2 (%)	ω_1(%)	d	Zmin (Ω)	Zmax (Ω)
10	38	0.621	29	133
15	45	0.713	33	111
50	70	0.711	41	77
61	94	0.764	52	140

To have a minimum characteristic impedance of 25 Ω and a maximum one of 140 Ω, the lowest bandwidth is around 10 % for ω_2 and the highest is around 95 % for ω_1.

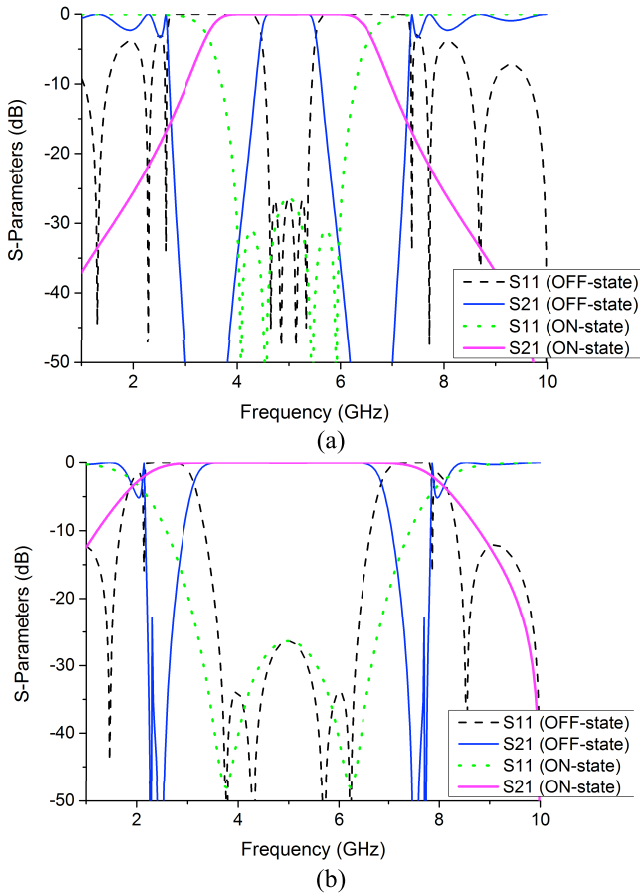

FIGURE 4. Examples of bandwidth switchable bandpass filter. (a) A 15 % relative bandwidth in OFF-state and a 45 % bandwidth in the ON-state. (b) A 61 % relative bandwidth in OFF-state and a 94 % bandwidth in the ON-state.

III. MANUFACTURING PROCESS

Therefore, the idea is to design switchable bandpass filters on a HR-Si substrate. It is doped with Boron (a P-Type substrate) with a resistivity of $\rho = 2500\ \Omega$.cm and a thickness of 675 μm. The tunability can be reached with integrated N^+PP^+ junctions in the substrate, using ScDDAs from the middle to the end of each stub allowing the stubs commutation from open-ended to short-ended, *i.e* from the OFF-state to the ON-state.

As described in Fig. 5, the fabrication process is based on classical steps of semiconductor components manufacturing. First, the wafer is oxidized on the two faces, then, the oxide on bottom face is removed in order to dope the wafer with boron atoms by ion implantation technique to obtain a surface concentration of a little bit over 10^{19} atoms/cm^3 with around a 3 μm depth. The doping allows to improve the ohmic contact between the silicon and the aluminum.

Next, on the top face, a photosensitive resin is deposited and then insolated through a chrome mask to allow the oxide etching followed by the resin removal. A silicon area is no longer protected and can therefore be doped with phosphorus atoms by solgel deposition (in order to reach a little bit over

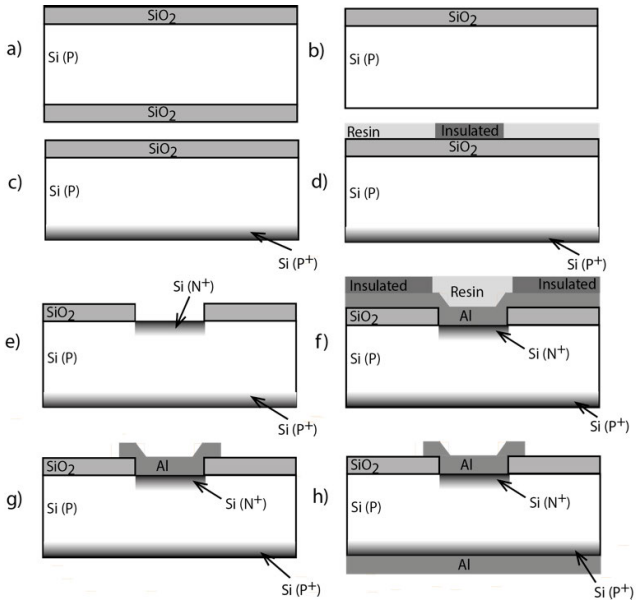

FIGURE 5. Fabrication process of the tunable filter based on ScDDAs. a) Oxidation of the P-type wafer on both faces. b) SiO2 etching on the bottom face. c) Bottom face P^+ implantation. d) Photoresist deposition and patterning on the top face. e) N^+ doping by solgel deposition and patterning. f) Aluminum and then photoresist deposition and patterning. g) Top face aluminum etching. h) Bottom face aluminum deposition.

10^{19} atoms/cm^3 of doping concentrations at the surface) to target doped areas with around a 3 μm depth. Then, the solgel is removed and after the doping steps, there is an aluminum deposition and a photolithography step before etching the aluminum on the top face. To finish the process, the resin is removed and the aluminum is deposited on the whole bottom face. Therefore, only two masks are necessary to manufacture the devices, the first one is for the top-face doping steps and the second one for the top-face metallization steps.

IV. MODELLING

The filter is switchable by using ScDDAs which are some integrated PIN diodes. They can be modeled by resistor in series with a capacitor when the junction is not biased or by a low resistor when the junction is forward biased (Fig. 6). In order to predict accurately the tunable devices behavior, the proposed simulation method takes place in three steps:

Firstly, the junctions manufacturing steps (time and temperature oxidation, implantation, diffusion, etching…) are simulated with Athena from Silvaco©.

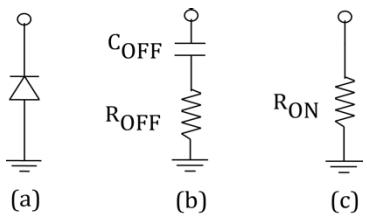

FIGURE 6. (a) PIN diode. (b) Equivalent electrical circuit without bias voltage. (c) Equivalent electrical circuit with a direct bias voltage.

This permits to calibrate the process in order to obtain the desired junctions (i.e. the atoms concentrations at the surface, the oxide and metallization thicknesses, the junction depths…).

Fig. 7 shows the Athena results of an N^+PP^+ junction, and this with an N^+ doped area width of 500 μm and a simulated area width of 1 mm. Fig. 8 illustrates the doping quantity (a) N^+ at the top face and (b) P^+ at the bottom face. A DC ground is connected to the backside of the junction (at the P^+ / aluminum contact) and the other electrode is connected to the top side (at the aluminum / N^+ contact) in order to simulate the electrical behavior of the junction.

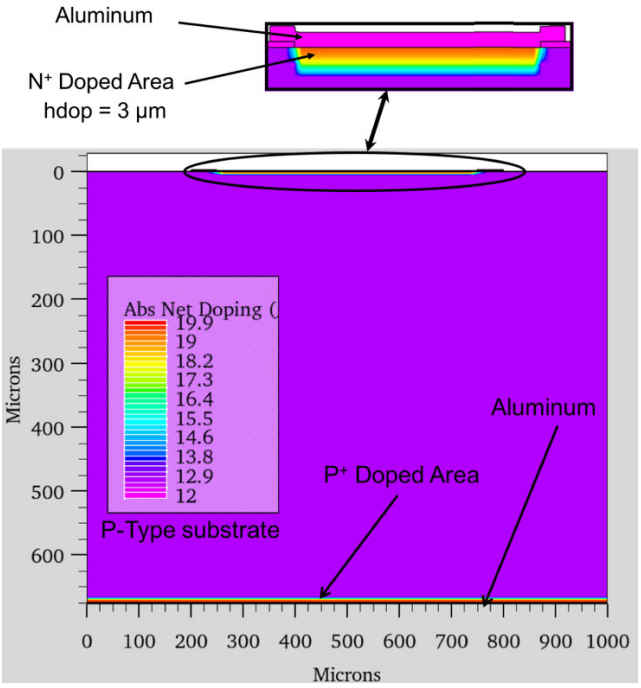

FIGURE 7. Doping quantity resulting from an Athena simulation of an N^+PP^+ junction.

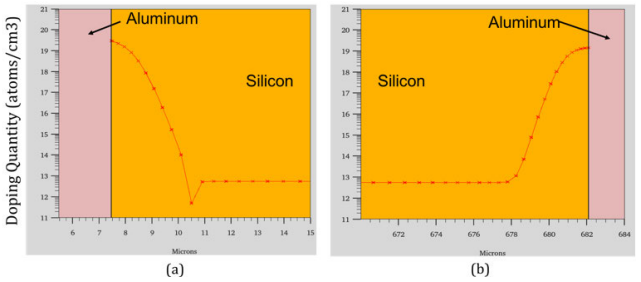

FIGURE 8. Athena simulation results of N^+PP^+ junction. (a) Top face doping quantity profile. (b) Bottom face doping quantity profile.

Secondly, the electrical junction characteristics are analyzed depending on the bias voltage with Atlas from Silvaco©, and the resistivity profiles of the junction (in the substrate thickness) are extracted depending on the voltage. Due to the N^+PP^+ junction used, the bias voltage has to be a negative one to forward bias the PIN diode.

With a bias voltage of 0 V, the resistivity is approximately equal to the substrate resistivity. The more the bias voltage decreases, the more the resistivity decreases. Table 3 summarizes the approximated resistivity values depending on the bias voltages when the junction is forward biased.

TABLE 3. Correspondence between the bias voltages and the resistivity values in the junction.

Bias voltage (V)	0	-0.5	-0.7	-0.9	-1	-1.3
Resistivity values (Ω.cm)	2500	15	5	1	0.8	0.1

Thirdly, when the N^+PP^+ junction is electrically simulated, the resistivity profiles are imported on the microwave design in the full wave HFSS^{TM} software to simulate its electromagnetic behavior. In this software, the main characteristics which define the materials properties are the permittivity and the conductivity for a conductive material or the loss tangent for a dielectric material.

In the case of the silicon (*i.e.* semiconductor material, with $\varepsilon_r = 11.9$), there are two possibilities: the first one is to consider that the conductivity is $\sigma = 0$ S/m and the loss tangent is evaluated at each frequency point using (24), where for both cases (ON- and OFF-states), the substrate resistivity ρ is equal to 2500 Ω.cm. In the ON-state, the resistivity in the junction (in the whole substrate height) is a low resistivity extracted from Atlas when it is forward biased.

$$\tan\delta = \frac{1}{\rho\omega\varepsilon_0\varepsilon_r} + 0.0018 \tag{24}$$

The second possibility is to include the resistivity values in the conductivity definition using (25) and to define the loss tangent as a constant using (26). The devices have been simulated with the loss tangent calculated at each frequency point (*i.e.* the first solution).

$$\sigma = \frac{100}{\rho}\ (\text{S/m}) \tag{25}$$

$$\tan\delta = 0.0018 \tag{26}$$

V. FOUR-POLE BANDWIDTH SWITCHABLE BANDPASS FILTER

To validate the co-design method permitting a switchable bandpass filter conception, a four-pole bandpass filter is analyzed. Thanks to the previous synthesis, this part details the design method, the simulated and the measured results. This demonstrator operates at 5 GHz and the bandwidths ω_2 and ω_1 are chosen equal to 0.5 and 0.7 in the OFF- and ON-states, respectively.

A. SIMULATIONS

Therefore, using the element values for a Tchebyscheff filter and the constant d fixed at 0.711 (chosen to have the best tradeoff between all the impedance values), the impedance

TABLE 4. Results of the impedance values.

Access	$Z_0 = 50\ \Omega$
Inverter 12 = Inverter 34	$Zi_{12} = Zi_{34} = 55\ \Omega$
Inverter 23	$Zi_{23} = 62\ \Omega$
Stub 1 = Stub 4	$Zp_1 = Zp_4 = 77\ \Omega$
	$Zs_1 = Zs_4 = 41\ \Omega$
Stub 2 = Stub 3	$Zp_2 = Zp_3 = 75\ \Omega$
	$Zs_2 = Zs_3 = 51\ \Omega$

values for each inverter and each resonator are calculated and summed up in Table 4.

Fig. 9 illustrates the four-pole filter designed with ideal transmission lines (a) with half-wavelength stubs terminated by open-circuits (OFF-state) and (b) with quarter-wavelength stubs terminated by short-circuits (ON-state).

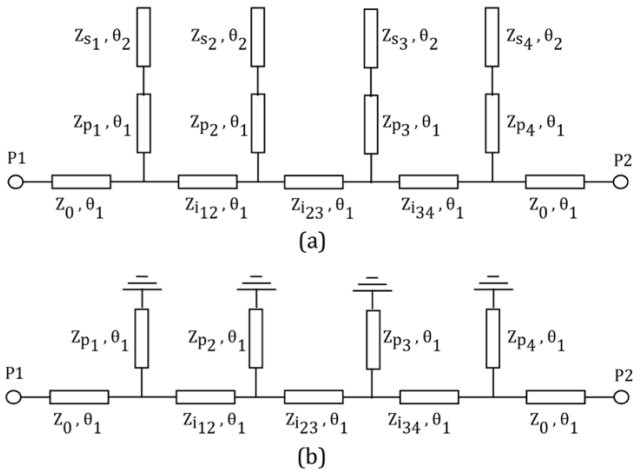

FIGURE 9. Ideal design of the four-pole switchable filter. (a) With half-wavelength open-circuited stubs (OFF-state). (b) With quarter-wavelength short-circuited stubs (ON-state).

The simulated results in the two-states obtained on ADS© from Keysight Technologies are presented in Fig. 10. The relative bandwidth switches from 50 %, *i.e.* a bandpass of 2.5 GHz from 3.75 GHz to 6.25 GHz, in the OFF-state, to 70 %, *i.e.* a bandpass of 3.5 GHZ from 3.25 GHz to 6.75 GHz, in the ON-state, and this with a constant central frequency equal to 5 GHz. These simulations validate the synthesis.

Then, to predict accurately the filter behavior in the two-states, this demonstrator (Fig. 11) is simulated using HFSS™. The ScDDAs are approximated as parallelepiped rectangles with the same surfaces as the doped areas, with the same resistivity as the substrate in the OFF-state (*i.e.* 2500 Ω.cm) and a low resistivity in the ON-state (*i.e.* 0.5 Ω.cm), and this in the whole substrate thickness. The ON-state resistivity is an average value that can be achieved with the characteristics of this junction.

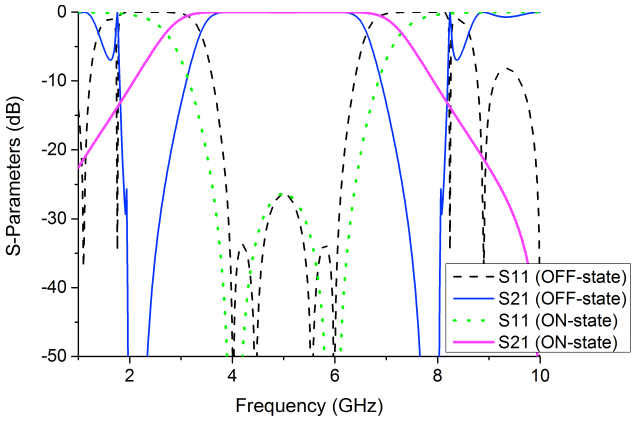

FIGURE 10. Ideal simulated results of the four-pole bandwidth switchable bandpass filter in the ON- and OFF- states.

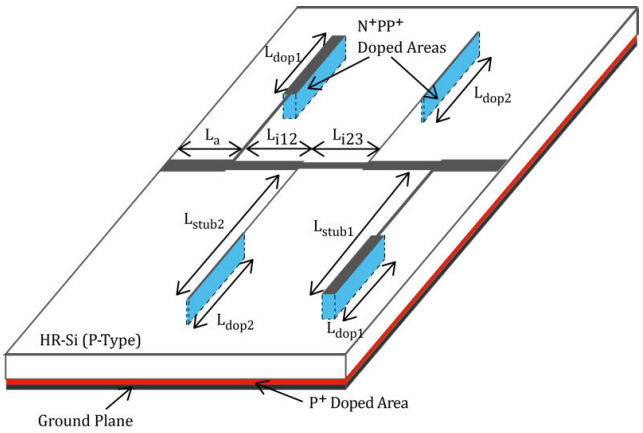

FIGURE 11. Design of the four-pole bandwidth switchable bandpass filter.

The lengths and the widths of each access lines, stubs and inverters are calculated thanks to the characteristic impedance values from the synthesis. The theoretical values are a little bit modified to take into account the technology (substrate and radiating effects). The dimensions of the four-pole switchable bandpass filter are listed in Table 5.

TABLE 5. Dimensions of the four-pole switchable bandpass filter.

Access	$L_a = 3.98$ mm	$W_a = 0.56$ mm
Inverter 12 = Inverter 34	$Li_{12} = Li_{34} = 5.5$ mm	$Wi_{12} = Wi_{34} = 0.42$ mm
Inverter 23	$Li_{23} = 5.32$ mm	$Wi_{23} = 0.3$ mm
Stub 1 = Stub 4	$Lp_1 = Lp_4 = 5.62$ mm	$Wp_1 = Wp_4 = 0.13$ mm
	$Ls_1 = Ls_4 = Ldop_1 = 5.31$ mm	$Ws_1 = Ws_4 = Wdop_1 = 0.85$ mm
Stub 2 = Stub 3	$Lp_2 = Lp_3 = 5.31$ mm	$Wp_2 = Wp_3 = 0.18$ mm
	$Ls_2 = Ls_3 = Ldop_2 = 5.28$ mm	$Ws_2 = Ws_3 = Wdop_2 = 0.62$ mm

W_x stand for each respected length.

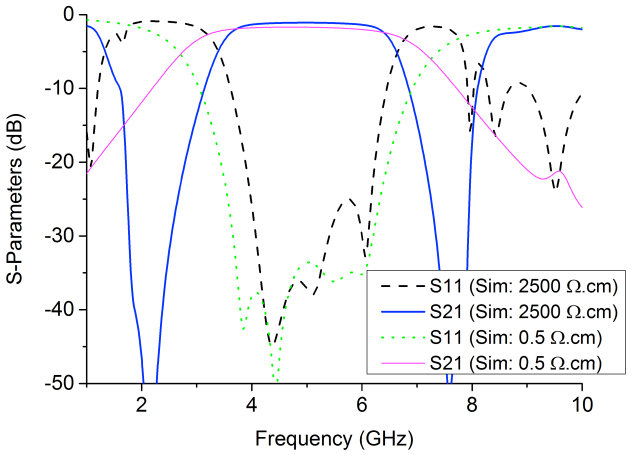

FIGURE 12. Simulated results of the four-pole bandwidth switchable bandpass filter in the ON- and OFF-states.

Fig. 12 shows the simulated results of the switchable bandpass filter in the two-states. The relative bandwidth switches from a 50 % bandwidth in the OFF-state with a central frequency equal to 5 GHz to a 70 % bandwidth in the ON-state with the same central frequency. The resistivity is of 2500 Ω.cm and 0.5 Ω.cm in the OFF- and ON-states respectively and the insertion losses are lower than 1.1 dB and 1.7 dB.

B. MEASUREMENTS

Fig. 13 shows the fabricated filter photograph and its environment. The filter has been measured with a 3680V Anritsu measuring cell and the results have been obtained using an R&S® ZVA 67 Vector Network Analyzer (VNA) connected to this cell. Then, a Short Open Load Through (SOLT) calibration has been performed in order to remove the cables losses. The DC ground is connected to the RF ground via the VNA, and the negative bias voltage (to forward bias the junctions) is applied with the RF signal.

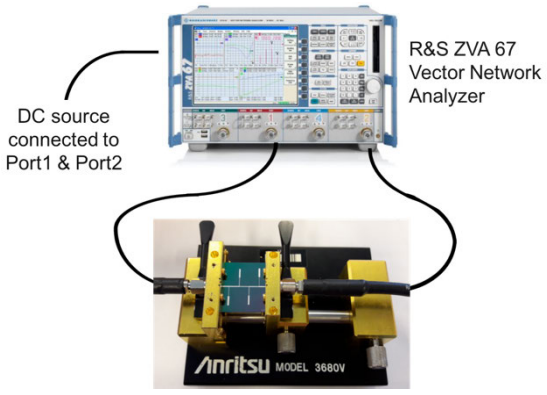

FIGURE 13. Photograph of the four-pole switchable bandpass filter and its environment.

The measured results are presented in Fig. 14. The filter switches from a 5 GHz bandpass filter with a 50 % bandwidth (without bias voltage) to a 5 GHz bandpass filter with a 70 % bandwidth (with a −1.65 V bias voltage), as predicted by the simulations. The insertion losses are lower than 3.7 dB and 1.6 dB in the ON- and OFF-state, respectively.

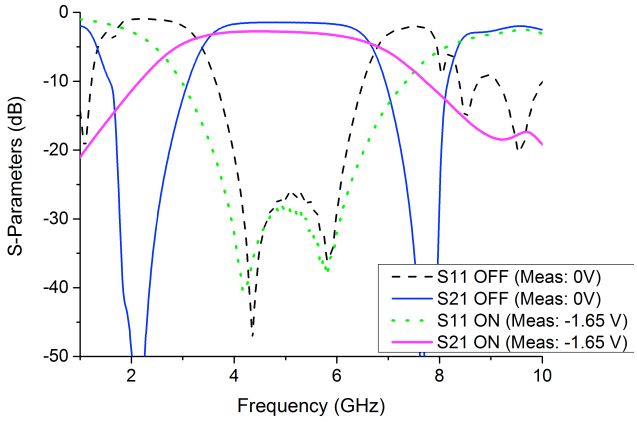

FIGURE 14. Measured results of the four-pole switchable filter in the ON- and OFF-states.

Fig. 15 and Fig. 16 compare the simulated results to the measured ones in the OFF- and ON-state. A good fit is obtained, despite an insertion loss level slightly higher than expected in the ON-state, this is due to the resistivity reached which is a little bit higher than 0.5 Ω.cm.

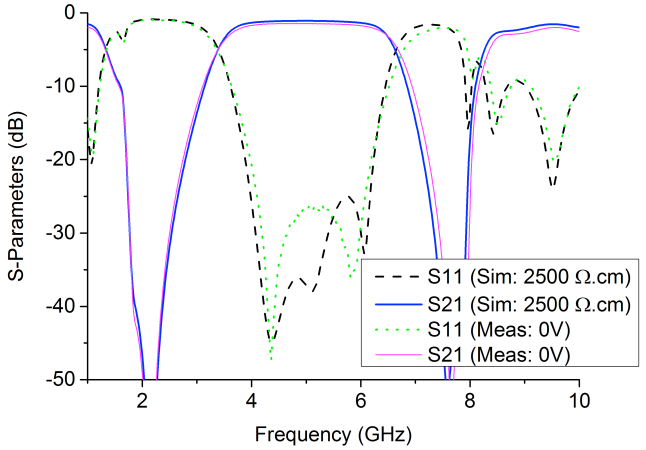

FIGURE 15. Comparison between the simulated and the measured results in the OFF-state.

Table 6 compares the proposed bandwidth switchable bandpass filter with some previous works related to a similar center frequency. The proposed filter offers similar performances, however, in previous works the parasitic effects of the p-i-n diodes, mounted on the substrate, limit the frequency rise. Thanks to the flexibility in the dimensioning and positioning of the ScDDAs, the dimensions and the absence of packaging will not bring parasitic effects with a frequency rise.

In the two states, the performances of our demonstrator could be improved with higher resistivity substrates. In the ON-state, a higher doping concentration or a reduced

TABLE 6. Comparison with previous work.

Ref.	Number of poles	Center Frequency (GHz)	Bandwidth (GHz)			Insertion Loss (dB)			Active elements	States-number	Number of active elements
			BW0	BW1	BW2	BW0	BW1	BW2			
[23]	3 / 1	1.5	50 %	29 %		0.9	1.1		p-i-n diodes	2	1
[24]	2	10	4.5 %	8.6 %		2.2	3.3		p-i-n diodes	2	1
[25]	4	10	15 %	5 %		≈ 2.5	≈ 4.5		p-i-n diodes	2	8
[26]	3	5.7	34.8 %	48.4 %	56.5 %	1.4	1.4	1.4	p-i-n diodes	3	4
[27]	2	1.9	35 %	16.3 %		0.4	4.17		p-i-n diodes	2	4
[27]	2	1.9	37.4 %	27.8 %		0.43	0.73		p-i-n diodes	2	4
This Work	4	5	50 %	70 %		1.45	2.8		Integrated junctions	2	4

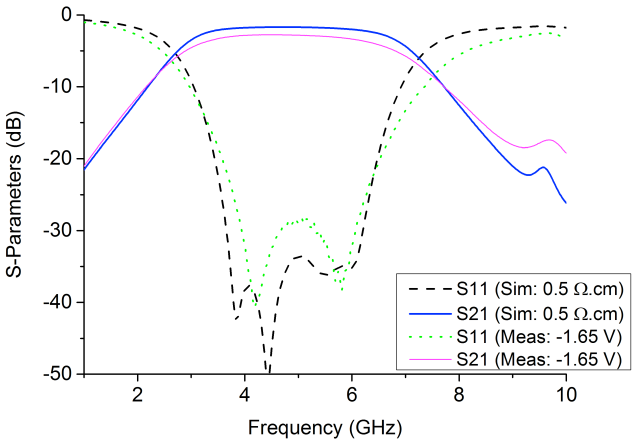

FIGURE 16. Comparison between the simulated and the measured results in the ON-state.

thickness under the doped areas will improve the filter quality factor.

VI. CONCLUSION

In this paper, a bandwidth switchable bandpass filter has been characterized from the synthesis to the measurement. It validates the co-design approach which allows the use of ScDDAs as integrated active elements to commute the resonators from half wavelength open-ended stubs to quarter wavelength short-circuited ones and therefore to switch the filter bandwidth. With this co-design approach, the mounted active components are no more needed, and their parasitic effects do no longer impact the filter performance and do no longer limit the frequency rise possibility. Moreover, the proposed synthesis permits to choose the two bandwidths in a large range, which has been validated by a demonstrator. The proposed filter is a 5 GHz four-pole bandpass filter with a bandwidth switching from 50 % in the OFF-state to 70 % in the ON-state. The simulated results fit well with the measurement results and even though the resistivity could be decreased in the ON-state to reduce the losses, the proposed co-design offers a great flexibility. If the substrate resistivity was of 10 kΩ.cm instead of 2.5 kΩ.cm, the insertion losses would be of 0.6 dB in the OFF-state. In the ON-state, with this substrate resistivity, if the resistivity in the junctions reached 0.1 Ω.cm (thanks to higher doping quantity), the insertion losses would decrease to 0.9 dB.

ACKNOWLEDGMENT

The authors would like to thank the TECHYP platform (the High Performance Computing Cluster of the Lab-STICC) thanks to which the devices could be simulated.

REFERENCES

[1] Y. Quere, C. Quendo, W. El Hajj, and C. Person, "A global synthesis tool and procedure for filter-antenna co-design," in *Proc. 15 Int. Symp. Antenna Technol. Appl. Electromagn.*, Jun. 2012, pp. 1–4.

[2] C. X. Mao1, S. Gao, Z. P. Wang, Y. Wang, F. Qin, B. Sanz-Izquierdo, and Q. X. Chu, "Integrated filtering-antenna with controllable frequency bandwidth," in *Proc. 9th Eur. Conf. Antennas Propag.*, Apr. 2015, pp. 1–4.

[3] S. Koley and D. Mitra, "A planar microstrip-fed tri-band filtering antenna for WLAN/WiMAX applications," *Microw. Opt. Technol. Lett.*, vol. 57, no. 1, pp. 233–237, Jan. 2015.

[4] M. E. Yassin, H. A. Mohamed, E. A. F. Abdallah, and H. S. El-Hennawy, "Circularly polarized wideband-to-narrowband switchable antenna," *IEEE Access*, vol. 7, pp. 36010–36018, 2019.

[5] J. Deng, S. Hou, L. Zhao, and L. Guo, "A reconfigurable filtering antenna with integrated bandpass filters for UWB/WLAN applications," *IEEE Trans. Antennas Propag.*, vol. 66, no. 1, pp. 401–404, Jan. 2018.

[6] X. Qing, C. Khan Goh, and Z. Ning Chen, "Impedance characterization of RFID tag antennas and application in tag co-design," *IEEE Trans. Microw. Theory Techn.*, vol. 57, no. 5, pp. 1268–1274, May 2009.

[7] G. Carchon, K. Vaesen, S. Brebels, W. De Raedt, E. Beyne, and B. Nauwelaers, "Multilayer thin-film MCM-D for the integration of high-performance RF and microwave circuits," *IEEE Trans. Compon. Packag. Technol.*, vol. 24, no. 3, pp. 510–519, 2001.

[8] I. Ju, R. L. Schmid, M.-K. Cho, S. Zeinolabedinzadeh, M. Mitchell, and J. D. Cressler, "Co-design of a SiGe BiCMOS X-band, asymmetric, low insertion loss, high power handling SPDT switch and an ultra low noise LNA for next-generation T/R modules," in *IEEE MTT-S Int. Microw. Symp. Dig.*, May 2016, pp. 1–4.

[9] A. Costanzo, M. Fabiani, A. Romani, D. Masotti, and V. Rizzoli, "Co-design of ultra-low power RF/Microwave receivers and converters for RFID and energy harvesting applications," in *IEEE MTT-S Int. Microw. Symp. Dig.*, May 2010, pp. 856–859.

[10] V. Rizzoli, A. Costanzo, E. Montanari, and P. Spadoni, "CAD procedures for the Nonlinear/Electromagnetic co-design of integrated microwave transmitters," in *IEEE MTT-S Int. Microw. Symp. Dig.*, Jun. 2007, pp. 2031–2034.

[11] D. Packiaraj, V. S. Reddy, G. J. D'Mello, and A. T. Kalghatgi, "Electronically switchable suspended substrate stripline filters," in *Proc. RF Microw. Conf.*, Oct. 2004, pp. 64–66.

[12] E. Fourn, C. Quendo, E. Rius, G. Tanne, C. Person, F. Huret, P. Blondy, A. Pothier, C. Champeaux, P. Tristant, and A. Catherinot, "Bandwidth and central frequency tunable bandpass filter," in *Proc. 32nd Eur. Microw. Conf.*, Oct. 2002, pp. 1–4.

[13] A. Ocera, P. Farinelli, P. Mezzanotte, R. Sorrentino, B. Margesin, and F. Giacomozzi, "A novel MEMS-tunable hairpin line filter on silicon substrate," in *Proc. Eur. Microw. Conf.*, Sep. 2006, pp. 803–806.
[14] D. Bouyge, D. Mardivirin, J. Bonache, A. Crunteanu, A. Pothier, M. Duran-Sindreu, P. Blondy, and F. Martin, "Split ring resonators (SRRs) based on micro-electro-mechanical deflectable cantilever-type rings: Application to tunable stopband filters," *IEEE Microw. Wireless Compon. Lett.*, vol. 21, no. 5, pp. 243–245, May 2011.
[15] A. Pothier, J.-C. Orlianges, G. Zheng, C. Champeaux, A. Catherinot, D. Cros, P. Blondy, and J. Papapolymerou, "Low-loss 2-bit tunable bandpass filters using MEMS DC contact switches," *IEEE Trans. Microw. Theory Techn.*, vol. 53, no. 1, pp. 354–360, Jan. 2005.
[16] Z. Brito-Brito, I. Llamas-Garro, G. Navarro-Munoz, J. Perruisseau-Carrier, and L. Pradell, "UMTS-WiFi switchable bandpass filter," in *Proc. 39th Eur. Microw. Conf.*, Sep. 2009, pp. 125–128.
[17] S. Sirci, J. D. Martinez, and V. E. Boria, "Low-loss 3-bit tunable SIW filter with PIN diodes and integrated bias network," in *Proc. 43rd Eur. Microw. Conf.*, Oct. 2013, pp. 1211–1214.
[18] M. Koochakzadeh and A. Abbaspour-Tamijani, "Switchable bandpass filter for 0.3-0.6 GHz," in *IEEE MTT-S Int. Microw. Symp. Dig.*, Jun. 2007, pp. 557–560.
[19] Z. Brito-Brito, I. Llamas-Garro, L. Pradell-Cara, and A. Corona-Chavez, "Microstrip switchable bandstop filter using PIN diodes with precise frequency and bandwidth control," in *Proc. 38th Eur. Microw. Conf.*, Oct. 2008, pp. 1707–1710.
[20] C. Lugo and J. Papapolymerou, "Electronic switchable bandpass filter using PIN diodes for wireless low cost system-on-a-package applications," *IEE Proc. Microw., Antennas Propag.*, vol. 151, no. 6, pp. 497–502, Dec. 2004.
[21] M. F. Karim, Y.-X. Guo, Z. N. Chen, and L. C. Ong, "Miniaturized reconfigurable and switchable filter from UWB to 2.4 GHz WLAN using PIN diodes," in *IEEE MTT-S Int. Microw. Symp. Dig.*, Jun. 2009, pp. 509–512.
[22] J. Lee, Z.-M. Tsai, and H. Wang, "A band-pass filter-integrated switch using field-effect transistors and its power analysis," in *IEEE MTT-S Int. Microw. Symp. Dig.*, 2006, pp. 768–771.
[23] W.-H. Tu, "Compact low-loss reconfigurable bandpass filter with switchable bandwidth," *IEEE Microw. Wireless Compon. Lett.*, vol. 20, no. 4, pp. 208–210, Apr. 2010.
[24] C. Lugo and J. Papapolymerou, "Single switch reconfigurable bandpass filter with variable bandwidth using a dual-mode triangular patch resonator," in *IEEE MTT-S Int. Microw. Symp. Dig.*, 2005, pp. 779–782.
[25] C. Rauscher, "Reconfigurable bandpass filter with a three-to-one switchable passband width," *IEEE Trans. Microw. Theory Techn.*, vol. 51, no. 2, pp. 573–577, Feb. 2003.
[26] T. Cheng and K.-W. Tam, "A wideband bandpass filter with reconfigurable bandwidth based on cross-shaped resonator," *IEEE Microw. Wireless Compon. Lett.*, vol. 27, no. 10, pp. 909–911, Oct. 2017.
[27] A. Miller and J.-S. Hong, "Wideband bandpass filter with reconfigurable bandwidth," *IEEE Microw. Wireless Compon. Lett.*, vol. 20, no. 1, pp. 28–30, Jan. 2010.
[28] C. Quendo, R. Allanic, D. Le Berre, and Y. Quere, "Novel approaches to design tunable devices," in *Proc. IEEE 18th Wireless Microw. Technol. Conf. (WAMICON)*, Apr. 2017, pp. 1–4.
[29] R. Allanic, Y. Quere, D. Le Berre, and C. Quendo, "A novel approach to co-design microwave devices with distributed switches," in *Proc. Asia–Pacific Microw. Conf. (APMC)*, Dec. 2016, pp. 1–4.
[30] R. Allanic, C. Quendo, Y. Quéré, and D. Le Berre, "Intrinsically microwave tunable resonator designed on silicon," *Electron. Lett.*, vol. 52, no. 20, pp. 1697–1699, Sep. 2016.
[31] R. Allanic, D. Le Berre, Y. Quere, C. Quendo, D. Chouteau, V. Grimal, D. Valente, and J. Billoue, "Three-state microwave tunable resonator integrating several active elements on silicon technology in a global design," *IEEE Microw. Wireless Compon. Lett.*, vol. 28, no. 2, pp. 141–143, Feb. 2018.
[32] R. Allanic, D. Le Berre, Y. Quere, C. Quendo, D. Chouteau, V. Grimal, D. Valente, and J. Billoue, "Continuously tunable resonator using a novel triangular doped area on a silicon substrate," *IEEE Microw. Wireless Compon. Lett.*, vol. 28, no. 12, pp. 1095–1097, Dec. 2018.
[33] C.-Y. Hung and M.-H. Weng, "Investigation of the silicon substrate with different substrate resistivities for integrated filters with excellent performance," *IEEE Trans. Electron Devices*, vol. 59, no. 4, pp. 1164–1171, Apr. 2012.
[34] R. Allanic, J. P. Cortes, J. Benedicto, D. Le Berre, Y. Quere, C. Quendo, D. Chouteau, V. Grimal, D. Valente, and J. Billoue, "Temperature dependence of tunable resonators on FR4 and silicon," in *Proc. IEEE Asia Pacific Microw. Conf. (APMC)*, Nov. 2017, pp. 1234–1237.
[35] G. L. Matthaei, L. Young, and E. M. T. Jones, *Microwave Filters, Impedance-Matching Networks, and Coupling Structures*, vol. 1. 1964.

ROZENN ALLANIC (Member, IEEE) received, after a successful resumption to studies, in 2009, the Electrical Engineer and Ph.D. degrees in electrical engineering from the University of Brest, France, in 2012 and 2015, respectively.

In 2016, she joined the Lab-STICC Group, University of Brest, as a Postdoctoral Researcher, to become a Researcher, in 2019. Her current research interests include modeling and co-design of tunable microwave devices (switches, filters, and antennas) on semiconductor substrates and multiphysics modeling. She also works on 2D and 3D antenna arrays for beam steering (in planar technology and additive manufacturing). She is also the Leader of the Fr/U.K. Research Project (MCM ITP An-DRO). She participates in several national projects. She was invited to present her works in the International Conference on Smart Materials, Structures and Systems, in 2017.

Dr. Allanic has served as the Session Chair for Asia Pacific Microwave Conference, in 2017 and 2018, and a Reviewer for the International Conferences, the *International Journal of Electronics, Microwave and Wireless Components Letters* and *Microwave Theory and Techniques*.

DENIS LE BERRE (Member, IEEE) received the Ph.D. degree in electrical engineering from the University of Brest, France, in 1997.

From 1997 to 2006, he was an Associate Professor with the Electronics Department, University of Brest. In 2006, he has joined the Engineering School (ESIAB), University of Brest. He currently carries out research at the Lab-STICC Laboratory, where his activities concern the modeling and design of microwave circuits and also optoelectronic systems.

YVES QUERE (Member, IEEE) is currently the UBO Open Factory Director and an Assistant Professor in electronics. His research interests include microwave antenna and sensor design, multiphysics modeling, and additive manufacturing. He is the Co-Founder and the Founder of three innovative entities, such as the Master of Engineering Program in Telecommunication, in 2013; the common laboratory called LATERAL with Thales Optronique, Paris, in 2016; and the Multi-Disciplinary Open Innovation Laboratory, UBO Open Factory, in 2015. These three entities are naturally interacting together through Open Innovation. He is the Leader of three Fr/U.K. research projects (MCM ITP PYRANA, COBRA, and LIZARD) and is participating in several national and international projects (ANR, CATRENE, and EURIPIDES). He was an Invited Researcher with NTU, Singapore, for six weeks, in 2013; and Cranfield University, U.K., for six months, in 2015.

CÉDRIC QUENDO (Senior Member, IEEE) received the Electrical Engineer degree and the Ph.D. degree in electrical engineering from the University of Brest, France, in 1999 and 2001, respectively.

From 2001 to 2010, he gave courses and conducted research in several institutes. Since 2010, he has been a Professor with the Electronic Department, University of Brest. From 2012 to 2016, he was the Vice-President of the University of Brest. Since 2017, he has been the Head of the Lab-STICC Laboratory, Microwaves Optoelectronics and Materials Group, (more than 100 persons), France. His research interests include modeling and design of microwave devices for microwave and millimeter-wave applications.

DAVID CHOUTEAU received the Master of Science degree in physics from the University of Orléans, Orléans, France, in 1997.

He joined the Laboratoire de Microélectronique et Microstructures, CNRS, Bagneux, France, in 1999, and the Laboratoire de Photonique et de Nanostructures, CNRS, Marcoussis, France, in 2001, where he was in charge of development for dielectric thin films deposition and characterization. He has been a Permanent Engineer with the Laboratory GREMAN, University of Tours/CNRS/INSA CVL, Tours, France, since 2014. He is in charge of photolithography processes and optical characterization at CERTeM platform.

VIRGINIE GRIMAL was born in Chartres, France, in 1978. She received the Ph.D. degree in materials physics from the University of Tours, in December 2005.

She completed her thesis at CEA (French Atomic Energy Commission), Monts, France. From 2006 to 2008, she was a Temporary Lecturer and a Researcher with the Science Faculty, University of Tours. Her research interests include hyperfrequency magnetoelastic effect on spinel ferrite. Her research was the effect on TiO2 nanoparticles synthesis on electron spin resonance. Since 2008, she has been a Researcher Engineer with the University of Tours. She works in microelectronics manufacturing. She works on thin layer deposition (plasma enhanced chemical vapor deposition, low-pressure chemical vapor deposition, and physical vapor deposition), thin layer etching (reactive ion etching, inductive coupled plasma, and ion beam etching), and X-ray diffraction.

DAMIEN VALENTE was born in Orléans, France, in 1983. He received the M.Sc. degree in electronic and microsystems engineering and the Ph.D. degree in microelectronic from the University of Tours, Tours, France, in 2006 and 2011, respectively.

Since 2011, he has been a Research Engineer with the GREMAN Laboratory (Research Group in Materials Microelectronics Acoustics and Nanotechnologies), UMR7347 CNRS, University of Tours. He is involved in the characterization of wide band gap and porous materials and devices.

JÉRÔME BILLOUE received the M.Sc. degree in telecommunications from the Université de Poitiers, France, in 2004, and the Ph.D. degree in electronic and engineer science form the Université de Tours, France, in 2007.

He is currently an Associate Professor with the GREMAN Laboratory, France, (Research Group specialized on materials, microelectronics, acoustics, and nanotechnology) in the Microelectronics Team. He is also the Deputy Director of the Laboratory. His current research interests include radio-frequency passive devices design, modeling, integration and characterization on new semiconductor materials for microelectronics, and the IoT.